SUPPLEMENTAL MATERIAL

Independent cross-checks have been performed at every step in the analysis, starting from the low-level image processing to the generation of the data pixel distribution, the identification of defects, the modeling of the DM signal, and the extraction of the DM signal upper limit. All of these checks yield consistent results.

Rates

The observed time dependence of the rate R_1^i is consistent with dark current stabilizing over time, characteristic in these types of devices. To confirm this interpretation we check the time dependence of the $2e^-$ rate, R_2^i, in the same data set. We sum the pixel charge distribution of 100 consecutive images to guarantee a sufficient number of pixels with $2e^-$ and then fit it with the sum of 3 Gaussians to obtain R_2^i. The exponential time decay constant for R_2^i, $\tau_{2e} = 35 \pm 24$ days, when compared with that for R_1^i is consistent with a Poisson process, as expected for dark current.

Model-independent search

A deviation from the null hypothesis (no modulation) is observed for T=26 h in the L-side. The best fit amplitude when fixing T=26 h is found to be $A = (594 \pm 103)$ events/g/day with a phase $\phi = (10.5 \pm 0.7)$ h. The best fit amplitude for T=24 h is found to be $A = (229 \pm 103)$ events/g/day with a phase $\phi = (6.7 \pm 1.7)$ h. This cannot be interpreted as evidence for a DM signal, not only because it does not match the expected period, but also because a much higher deviation should have been found in the U-side, which accounts for 70% of the data. In fact, for the U-side, the best fit point for amplitudes and phases is $A = (141 \pm 42)$ events/g/day and $\phi = (7.7 \pm 1.2)$ h when T=26 h. For T=24 h, instead, $A = (121 \pm 42)$ events/g/day and $\phi = (16.8 \pm 1.3)$ h. The same argument is valid for changes in external parameters like the temperature, which should affect the measured rate in both the U and L-side. Also, no modulation is found in relevant slow control data (several temperature sensors in the apparatus and cryocooler parameters). Applying the same model-independent search on the data set previously excluded due to the presence of serial register traps (which should have no effect on a possible modulation signal), no evidence for a T=26 h signal is found. Note that the L-side data consists of pixels close to the amplifier (columns > 74 are rejected), and the modulation amplitude is reduced by a factor of two when all columns are included. From these observations, an instrumental effect limited to the amplifier on the L side is likely the origin of the deviation. Note that since we took data for over two months a T=26 h modulation is washed out when searching for a signal at a sidereal period (23.93 h), hence we do not expect any significant effect on the DM-e^- scattering analysis. Indeed, excluding the L-side data changes the exclusion limits in Fig. 4 by at most 5% (12%) for the ultralight (heavy) mediator. As our primary objective is to assess the temporal stability of the detector by quantifying the statistical significances of fluctuations in the data, the presence of a modulated signal highlights the complexity of the detector's time dependence. We acknowledge the need for a comprehensive understanding of these temporal variations. To address this, the method outlined involves a comparison of best-fit amplitudes and phases across different amplifiers or CCDs. This cross-check enables us to discern any signal origin that might be common to all CCDs, aiding in the ongoing effort to refine our understanding of the detector's time-dependent behavior and ensuring the robustness of our results against potential instrumental artifacts in future searches.

Exclusion limits

For the model-independent analysis, we have performed toy-MC simulations under H_0 (no modulation), finding that the test statistic t_q asymptotically follows a χ^2 distribution with two degrees of freedom.

We have also verified that our limits in Fig. 4 have the correct coverage by performing the analysis on toy Monte Carlo simulations, which include both a signal and background. We find that the signal is properly rejected or discovered according to our 90% C.L.

In Fig. 5 we show the estimated sensitivity bands. The bands are obtained from 10000 pseudo data sets constructed by randomly shuffling the time of the images. The shuffling method guarantees that no modulation is present in the pseudo data set and takes into account the uncertainty in the measured rates. A 90% C.L upper limit is then calculated for each pseudo data set, and sensitivity bands are derived from the distribution of these upper limits. The limit reported in Fig. 4 falls in the 2σ (95.4%) sensitivity band.

We also perform a cross-check of the exclusion limits with a less sensitive but simpler method by computing the correlation

$$\rho = \frac{\sqrt{2}}{N_{\rm im}||R_1||} \sum_{i=1}^{N_{\rm im}} R_1^i \cos\left[\frac{2\pi(t_i - \phi)}{T}\right], \qquad (1)$$

where $||R_1|| = \sqrt{\sum_{i=1}^{N_{\rm im}} (R_1^i)^2 / N_{\rm im}}$ and T and ϕ are fixed to the period and phase predicted by the DM-e^- scattering model described in the main text. The probability distribution of ρ is obtained from toy Monte Carlo simulations, which include only the background model, and

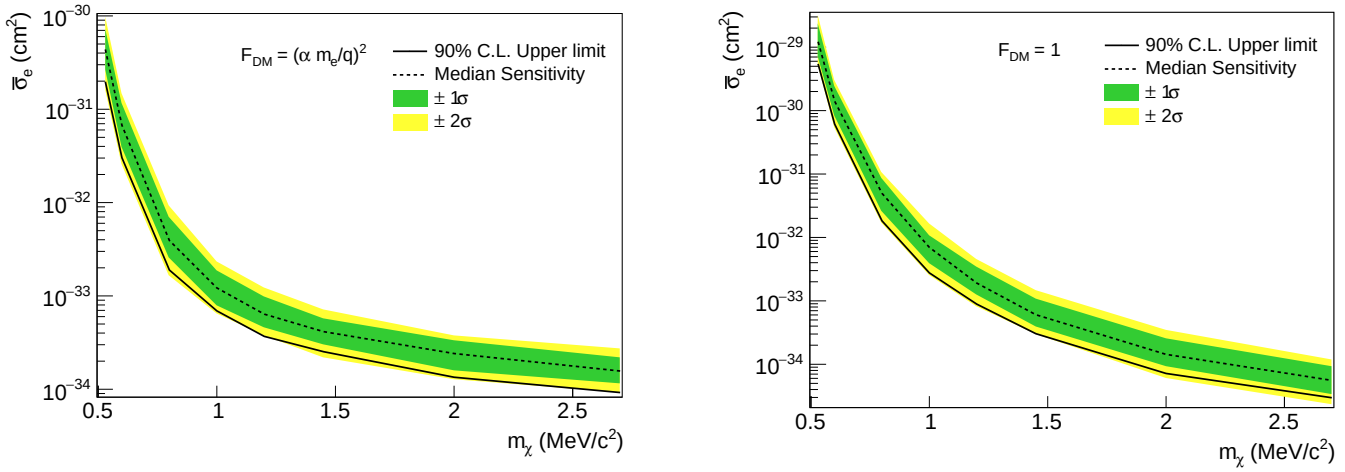

FIG. 1. Sensitivity bands for DM-electron interactions via a ultralight (left) and heavy (right) mediator. Also shown is the median sensitivity (dashed line) and the DAMIC-M upper limit from Fig. 4 (solid line).

then used to derive a 90% limit on the amplitude of a putative daily modulation signal. We convert the rate to cross section using Eq. (2). The corresponding exclusion limits are a factor of 1.2 weaker than the nominal limits obtained from the likelihood.

In Fig. 6 we present DAMIC-M 90% C.L. exclusion limits for ultralight (left) and heavy (right) mediators up to masses of 1000 MeV/c^2, obtained by combining results in Fig. 4 with our previous limits [16].

Theoretical uncertainties

We use `QEDark` as the reference theoretical model for proper comparison with previous and forthcoming results from other experiments. We note that theoretical uncertainties are significant for DM masses below 2.7 MeV/c^2, with `QEDark`-based limits almost a factor 100 better than those obtained with `DarkELF` [83] and `EXCEED-DM` [84, 85] models (see Supplemental Material of Ref. [16].)

Earth-scattering calculations

The velocity distribution at the detector was determined with an updated version of the VERNE code to take into account Earth-scattering effects. This code will be described in full in a future publication (Ref. [62]). Here we provide a brief summary of the calculation, including signal rates and modulation amplitude for a number of benchmark parameter points, and a comparison with other Earth-scattering calculations available in the literature.

The original VERNE code [60], described in Ref. [59], was tailored to the Earth-scattering of heavy DM particles. It assumed straight-line trajectories for the incoming DM particles and a continuous energy loss due to scattering with nuclei in the atmosphere and Earth. Instead, light DM ($m_\chi \ll m_N$) may be deflected substantially when scattering off a nucleus of mass m_N, while the energy losses in a single scattering event (proportional to m_χ/m_N) are typically negligible. The updated version of VERNE used in the present work assumes that the DM particles follow a straight-line trajectory until they scatter, at which point they either continue along the same trajectory, or they are reflected back along the incoming trajectory with probability $p_{\rm back}$. The value of $p_{\rm back}$ depends on the type of DM interaction and a suitable estimate can be calculated as the fraction of scattering events which deflect the DM particle into the backwards hemisphere. We fix $p_{\rm back} = 0.875$ and $p_{\rm back} = 0.5$ for the light and heavy mediator cases respectively. We assume zero energy loss with each scattering and take into account up to two scattering events for each incoming trajectory. The flux at the detector is given by the sum of those particles which arrive at the detector without being reflected out to space and those particles which are reflected back to the detector, having already passed the detector. Full details of the formalism and implementation will appear in Ref. [62].

In Fig. 7 we compare the VERNE DM velocity distributions at the detector with those obtained when the Earth-scattering effects are calculated using DAMASCUS [53, 86, 87], a more accurate but computationally demanding 3D Monte Carlo simulation. The simplified approach adopted in VERNE reproduces to better than 20% the DAMASCUS predictions. We have repeated our analysis at a DM mass of 1 MeV/c^2 using the DAMASCUS code; the corresponding limits differ from those obtained with VERNE by less than 30%. The use of VERNE has also allowed for a number of additional checks. In the VERNE calculation of the DM velocity distribution

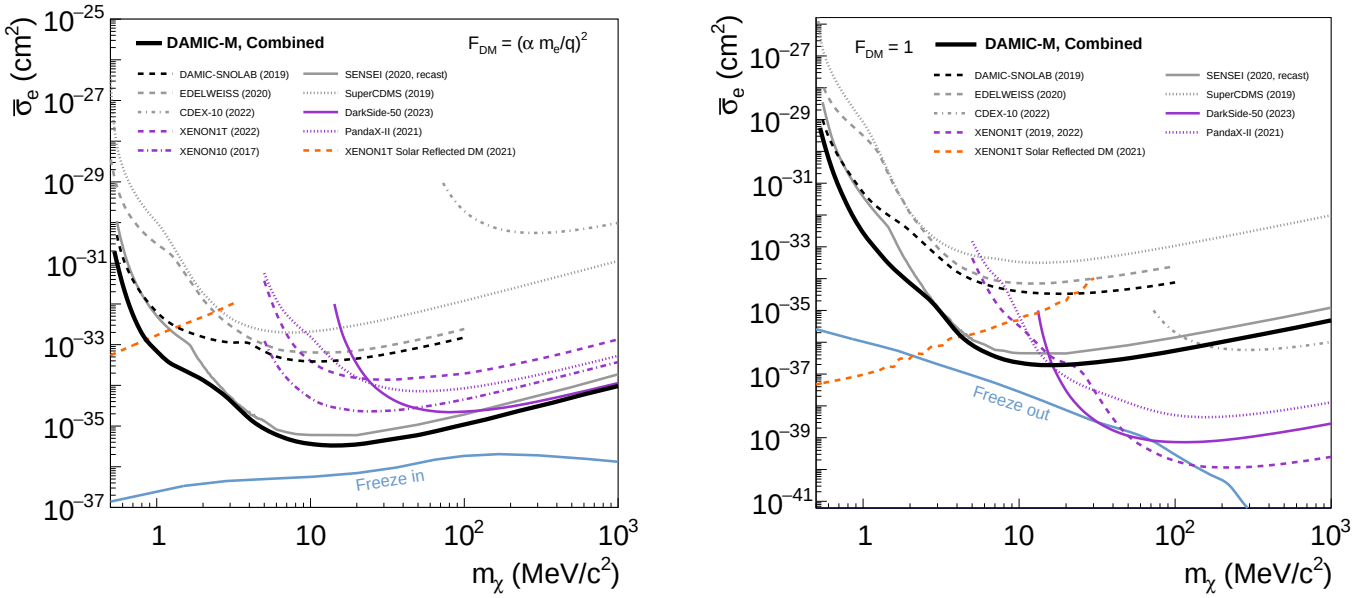

FIG. 2. DAMIC-M 90% C.L. upper limits (solid thick black) on DM-electron interactions through an ultralight (left) and heavy (right) dark photon mediator obtained combining the daily modulation analysis with the previous DAMIC-M result [16]. Also shown are previous limits from other experiments: DAMIC-SNOLAB [13] (dashed black); SENSEI [14, 64] (solid gray); EDELWEISS [15] (dashed gray); SuperCDMS [12] (dotted gray); CDEX-10 [81] (dot-dashed gray); DarkSide-50 [82] (solid violet); XENON1T combined result from [65, 66] (dashed violet); PandaX-II [67] (dotted violet); a limit obtained from XENON10 data in Ref. [68] (dash-dotted violet); and a limit obtained from XENON1T data considering "solar reflected DM" (dashed orange) from Ref. [69] (left) and Ref. [70] (right). Theoretical expectations assuming a DM relic abundance from freeze-in and freeze-out mechanisms are also shown in light blue [71].

the Earth's speed is fixed to 263 km/s. To check the effect of this assumption we repeat the analysis using the largest and smallest value of v_E, 267 and 258 km/s, corresponding to the beginning and the end of the data-taking period. The exclusion limits change by at most 15%.

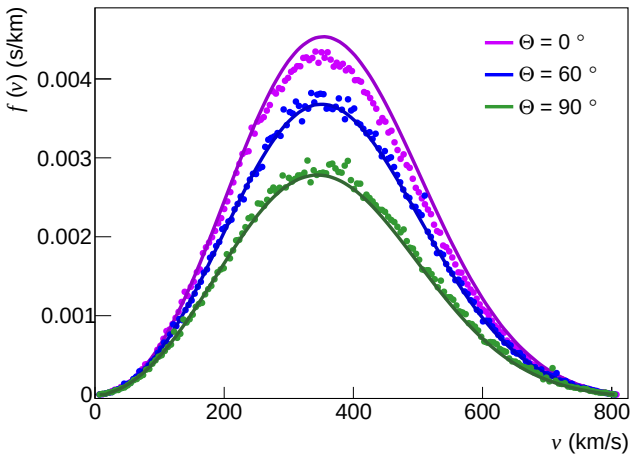

FIG. 3. Speed distributions at different isodetection angles for DM particles of mass 1 MeV/c^2 interacting via an ultralight dark photon mediator (VERNE, solid line; DAMASCUS, dots). The distributions are calculated for $\bar{\sigma}_e = 10^{-33}$ cm^2, close to the DAMIC-M limit at m_χ=1 MeV/c^2 reported in this letter.

For illustration, we report in Table I and II the mean DM-electron signal rate $\langle R \rangle$ and the amplitude A of the daily modulation, calculated using VERNE and DAMASCUS. The values are obtained for representative DM masses m_χ, and for cross sections $\bar{\sigma}_e$ close to the upper limits reported in Fig. 4. We find that the maximum difference between the two calculations is 32% for the modulation amplitude and 5% for the mean rate.

m_χ (MeV)	$\bar{\sigma}_e$ [cm^2]	A_D ($\frac{\text{events}}{\text{g·day}}$)	A_V ($\frac{\text{events}}{\text{g·day}}$)	$\langle R_D \rangle$ ($\frac{\text{events}}{\text{g·day}}$)	$\langle R_V \rangle$ ($\frac{\text{events}}{\text{g·day}}$)
0.53	10^{-31}	20	20	34	34
1.0	10^{-33}	45	51	150	157
2.7	10^{-34}	22	29	185	178

TABLE I. Modulation amplitude A and mean DM-electron signal rate $\langle R \rangle$ calculated with VERNE (V) and DaMaSCUS (D) for the ultralight mediator model. The mean $\langle R \rangle$ is obtained by averaging the rate over time. The modulation amplitude is defined as the maximum deviation from the mean rate, $A = \max(R^{max} - \langle R \rangle, \langle R \rangle - R^{min})$, for the first day of data taking. We use this amplitude definition because the daily modulation is not symmetric with respect to the mean rate.

m_χ (MeV)	$\bar{\sigma}_e$ [cm^2]	A_D ($\frac{\text{events}}{\text{g·day}}$)	A_V ($\frac{\text{events}}{\text{g·day}}$)	$\langle R_D \rangle$ ($\frac{\text{events}}{\text{g·day}}$)	$\langle R_V \rangle$ ($\frac{\text{events}}{\text{g·day}}$)
0.53	10^{-30}	6	6	10	11
1.0	10^{-32}	135	130	278	273
2.7	10^{-35}	6	7	25	26

TABLE II. The explanation can be found in Tab. I